

**Field Effect Transistors Based on Polycyclic Aromatic  
Hydrocarbons for the Detection and Classification of Volatile  
Organic Compounds**

Journal:	<i>ACS Applied Materials &amp; Interfaces</i>
Manuscript ID:	am-2013-005144.R1
Manuscript Type:	Article
Date Submitted by the Author:	14-Mar-2013
Complete List of Authors:	Bayn, Alona; Technion - Israel Institute of Technology, Department of Chemical Engineering Feng, Xinliang; Max-Planck Institute for Polymer Research, Synthetic Chemistry Mullen, Klaus; Max-Planck-Institute for Polymer Research, Haick, Hossam; Technion - Israel Institute of Technology, Department of Chemical Engineering

SCHOLARONE™  
Manuscripts

# Field Effect Transistors Based on Polycyclic Aromatic Hydrocarbons for the Detection and Classification of Volatile Organic Compounds

Alona Bayn,<sup>⊥</sup> Xinliang Feng,<sup>§</sup> Klaus Müllen,<sup>§</sup> and Hossam Haick\*,<sup>⊥</sup>

<sup>⊥</sup> *The Department of Chemical Engineering and the Russell Berrie Nanotechnology Institute, Technion – Israel Institute of Technology, Haifa 32000, Israel*

<sup>§</sup> *Max-Planck-Institute for Polymer Research, Postfach 3148, D-55021 Mainz, Germany*

## ABSTRACT

Polycyclic aromatic hydrocarbon (PAH) based field effect transistor (FET) arrays show great promise for detecting various chemical species. Here we present silane-modified PAH-FETs that can detect volatile organic compounds (VOCs) under confounding humidity conditions. We demonstrate the ability of PAH-FET sensor arrays in conjunction with statistical pattern recognition methods to (i) discriminate between aromatic and non-aromatic VOCs; (ii) distinguish polar and non-polar non-aromatic compounds and (ii) identify specific VOCs within the sub-groups (i.e., aromatic compounds, polar non-aromatic compounds, non-polar non-aromatic compounds). We further study the effect of water vapor on the sensor array's discriminative ability and derive patterns that are stable when exposed to different constant values of background humidity. Patterns based on different independent electronic features from an array of PAH-FETs may bring us one step closer to creating a unique fingerprint for individual VOCs in real-world applications in atmospheres with varying levels of humidity.

**KEYWORDS:** Polycyclic aromatic hydrocarbon; sensor; volatile organic compound; humidity; field effect transistor; detection.

## INTRODUCTION

1  
2  
3  
4  
5  
6 Volatile organic compounds (VOCs) tend to evaporate easily at room temperature. Many VOCs  
7  
8 are associated with emissions from industrial processes (*e.g.*, heating oil, aldehydes, alcohols),  
9  
10 transportation (*e.g.*, gasoline, diesel, kerosene) and use of organic solvents (*e.g.*, benzene,  
11  
12 butadiene, hexane, toluene, xylene, acetone) that are in part toxic or carcinogenic.<sup>1, 2</sup>  
13  
14 Furthermore, several VOCs associated with metabolic and/or pathophysiologic processes have  
15  
16 been used for diagnosing a wide variety of diseases, including, but not confined to, lung cancer,<sup>3-</sup>  
17  
18 <sup>11</sup> head and neck cancer,<sup>9</sup> liver metastasis,<sup>12</sup> kidney disease,<sup>13, 14</sup> Parkinson's disease and  
19  
20 Alzheimer's disease,<sup>15, 16</sup> and multiple sclerosis.<sup>17</sup> Diagnostic use of VOCs has led to increasing  
21  
22 the requirements for their detection and classification.  
23  
24  
25

26  
27 Detection of VOCs is generally achieved by means of gas sensors.<sup>18</sup> Although highly  
28  
29 selective sensors do exist for a limited number of substances (*e.g.*, hydrogen sulfide, phosphine),  
30  
31 such gas sensors are very sensitive to cross-interfering substances and provide an overall result in  
32  
33 response to a general class or group of chemically related contaminants. These gas sensors  
34  
35 provide a single collective reading for all of the detectable substances present in the surrounding  
36  
37 environment at any moment, but they cannot distinguish between the different contaminants they  
38  
39 are able to detect. Additionally, such gas sensors are highly affected by the humidity in the  
40  
41 environment examined.<sup>19-21</sup> Varying levels of humidity are a serious obstacle in the application of  
42  
43 sensors, causing different responses and leading to a decrease in the selectivity towards the  
44  
45 targeted analytes. Interaction between the water molecules and the charge carriers in the  
46  
47 semiconductor as well as their diffusion in grain boundaries,<sup>22</sup> causes change in the  
48  
49 intermolecular interactions, and in some cases, the influence of water associated ions and  
50  
51 molecules change the work function and morphology<sup>23</sup>. All the mechanisms noted affect the  
52  
53 electrical behavior of the sensor. The higher the humidity levels, the higher the deterioration  
54  
55  
56  
57  
58  
59  
60

1  
2  
3 effect of the sensors. There have been many attempts to overcome this complication.  
4  
5 Representative examples include the use of sensing materials that are not affected by changes in  
6  
7 humidity, or the use of several sensors reacting differently to water vapor in order to calibrate the  
8  
9 response to the analyte alone.<sup>23</sup> Unfortunately, the proposed approaches are applied on a sensor  
10  
11 created to identify one specific analyte. When dealing with an array of different sensors meant to  
12  
13 recognize a number of complex compounds, these approaches are harder to implement.<sup>24</sup> A novel  
14  
15 solution to the humidity problem suggested using FRID wireless sensors that provide a reliable  
16  
17 response in the presence of various humidity levels by a multivariate analysis from a single  
18  
19 sensor correcting the humidity effect. Nevertheless, wireless sensor networks are relatively new  
20  
21 technology, thus problems in maintenance, routing and coverage may present a challenge.<sup>25</sup> *With*  
22  
23 *this in mind, a simple and easy-to-use array of sensors that is minimally affected by*  
24  
25 *counteracting humidity background is definitely needed.*  
26  
27  
28  
29  
30

31  
32 To achieve chemical sensors with low sensitivity to humidity, we have recently exploited  
33  
34 Polycyclic Aromatic Hydrocarbons (PAH) derivatives.<sup>26-29</sup> PAH derivatives with hydrophobic  
35  
36 terminations produced a hydrophobic surface that effectively counteracted the sensitivity to  
37  
38 humidity, enabling detection of traces of VOCs even in high humidity environments (~ 80%  
39  
40 relative humidity).<sup>26-29</sup> In a series of preliminary studies, hybrid structures containing PAH layers  
41  
42 on top of a quasi 2D network of single wall carbon nanotubes (SWCNTs) have shown excellent  
43  
44 detection and classification of VOCs under both low and high humidity backgrounds. In these  
45  
46 devices, the PAH derivatives served as an electrically **insulating** adsorption phase for VOCs,  
47  
48 while the SWCNTs served as sole pathway for translating and transferring the PAH-VOC  
49  
50 interactions to electrical signals. Using this architecture, Zilberman et al. found that both the PAH  
51  
52 corona and the organic functionalities of these molecules contribute to the chemical sensing of  
53  
54 the VOCs.<sup>27</sup> For instance, the PAH corona, made of condensed aromatic rings, interacts strongly  
55  
56  
57  
58  
59  
60

1  
2  
3 with the phenyl rings of aromatic hydrocarbons (*e.g.*, ethylbenzene), while the detection of OH-  
4 terminated (polar) VOCs is promoted by the presence of oxygen in the substituent functionality.<sup>27</sup>  
5  
6 Nevertheless, in this architecture, the affinity of the PAH derivatives toward the VOCs of interest  
7  
8 can be finely tuned by proper selection of the (synthetically designed) PAH derivatives structures  
9  
10 – a process that requires continuous synthetic skills and efforts. Additionally, the involvement of  
11  
12 random network of SWCNTs might lead to relatively high production costs and might delay the  
13  
14 implementation of the PAH-based sensors in the well-established VLSI industry and/or  
15  
16 production lines.  
17  
18  
19  
20  
21

22 In this paper, we present a technology based on an array of field effect transistors (FETs)  
23 coated with a layer of different (semi-)conducting PAHs, **without** the involvement of any other  
24 (*e.g.*, SWCNT) conductive layer. PAH molecules are able to self-assemble into long molecular  
25 stacks with a large, electron-rich, semiconducting core, guaranteeing good charge carrier  
26 transport along the molecular stacking direction and a relatively insulating periphery.  
27  
28  
29  
30  
31  
32  
33

34 We investigate the possibility of using PAH-FETs as a fast, non-invasive portable  
35 technology that can be used for the widespread detection of various VOCs. In this endeavor, we  
36 examine the use of different electrical features extracted from a single sensor to increase the  
37 chances of correct identification (*cf.* refs. <sup>30, 31</sup>). Based on these results, we explore the optimal  
38 ways to utilize independent electrical parameters (*e.g.*, threshold voltage, mobility,  $I_{on/off}$  ratio) of  
39 PAH-FETs for the classification of various VOCs in a humid atmosphere while employing the  
40 analysis on an array of different sensors. We show that a combination of different electrical  
41 parameters, extracted from a single PAH-FET or from several devices, can be used as an array of  
42 virtual sensors.  
43  
44  
45  
46  
47  
48  
49  
50  
51  
52  
53  
54  
55  
56  
57  
58  
59  
60

## EXPERIMENTAL SECTION

**Device Preparation:** Back-gated PAH-FETs were deposited on a p-type Si (100) wafer covered with a 300 nm thick thermally grown SiO<sub>2</sub> field oxide layer (Figure 1a). Ten pairs of interdigitated Au/Ti electrodes with a circular geometry (overall radius of 1500 μm) were deposited on top of the SiO<sub>2</sub> layer and an aluminum back gate was deposited on the back face of the Si substrate after removal of the oxide from the back of the wafer. The width of each electrode was 5 μm, the thickness of each electrode was 250 nm, and the distance between the adjacent electrodes was 25 μm. The SiO<sub>2</sub> surface between the electrodes was functionalized with a hexyltrichlorosilane (HTS) monolayer using the two-step amine-promoted procedure described elsewhere.<sup>32-37</sup> Similar devices without the HTS layer were fabricated as controls. The HTS-terminated and pristine SiO<sub>2</sub> surfaces were spray coated with seven different PAH films that were chosen from a reservoir of seven PAH derivatives (*see* Figure 1b and Table 1). The synthesis of PAH-1<sup>38</sup>, PAH-2<sup>39</sup>, and PAH-7<sup>40</sup> and has been described in previous works. The synthesis of PAH-3 to PAH-6 will be described elsewhere. The PAH layer was spray-coated from a 50 μL 10<sup>-3</sup> M solution (PAH-2, PAH-3, and PAH-7 in toluene; PAH-4 in tetrahydrofuran), after which the devices were dried overnight in a 100 °C oven, to evaporate possible residual solvents in the PAH layer. Layer morphology and surface coverage were studied by scanning electron microscopy (SEM).

**Electrical FET Characterization in Air:** A probe station that is connected to a device analyzer (Agilent B1500A) was used to collect the electrical signals of the sensors in ambient air. Voltage-dependent back-gate measurements ( $I_{ds}$  vs.  $V_g$ ), swept backward and forward between -40 V and 40 V with 500 mV steps and at 30 V source-drain voltage ( $V_{ds}$ ), were used to determine the performance of the PAH-FET devices.

1  
2  
3 ***Sensing Volatile Organic Compounds:*** The PAH-FETs were exposed to three groups of VOCs:  
4  
5 alcohols (decanol and octanol), alkanes (hexane, decane and octane), and aromatic compounds  
6  
7 (mesitylene, styrene, ethyl benzene, and toluene). All compounds were purchased from Sigma  
8  
9 Aldrich Ltd. (Israel) and Fluka Ltd. (Israel), having >99% purity and <0.001% water. Table 2  
10  
11 lists the properties of the different analytes. Oil-free purified air, obtained from a compressed air  
12  
13 source, that had a baseline RH (relative humidity) of  $5.0 \pm 0.2\%$  and an organic contamination of  
14  
15 <0.3 ppm (measured by a commercial PID detector - ppbRAE 3000), was used as a carrier gas  
16  
17 for the analytes and as reference gas. The vapor of the analytes was created by a bubbler system  
18  
19 that uses glass bubblers, holding the analytes in liquid states. The saturated analyte vapor from  
20  
21 the bubblers was diluted with different flow rates of air to create different concentrations. The  
22  
23 relative humidity (RH) was regulated by a combination of dry air (5% RH) and water saturated  
24  
25 vapor (100% RH). The partial pressure of analyte vapors was changed between  $p_a/p_o = 0.05, 0.1$   
26  
27 and  $0.2$  ( $p_a$  stands for the partial pressure of the analyte and  $p_o$  stands for the saturated vapor  
28  
29 pressure at  $20^\circ\text{C}$ ) in an environment of 5% RH to 40% RH. Unless otherwise stated, we focus our  
30  
31 presentation on analytes at  $p_a/p_o = 0.1$  in an environment of either 5% RH or 40%RH. The  
32  
33 exposures were performed as follows: **(i)** exposure to dry air (5% RH) for 30 min; **(ii)** exposure  
34  
35 to VOC(s) for 20 min; **(iii)** cleaning the sensor surrounding with dry air for another 30 min. Two  
36  
37 repetitions per exposure were performed to ensure the reproducibility of the responses. The  
38  
39 electrical measurements of the PAH-FETs were conducted using a homemade exposure system.  
40  
41 The sensors developed were placed on a circuit board inside a stainless steel exposure chamber.  
42  
43 The electrical response of the sensors was measured by a Keithley 2636A system SourceMeter  
44  
45 and Keithley 3706 system Switch/Multimeter. S/D (S-source, D-drain) current ( $I_{ds}$ ) versus  
46  
47 voltage dependent back-gate ( $V_g$ ) measurements, swept backward between +40 V to -40 V with  
48  
49 200 mV steps and at  $V_{ds} = 30$  V, were performed.  
50  
51  
52  
53  
54  
55  
56  
57  
58  
59  
60

1  
2  
3  
4  
5  
6 **Data Analysis:** Four device features were extracted from each sensor by plotting the value of  
7  
8 each feature as a function of time and extracting the normalized response of the features. The four  
9  
10 normalized features examined in the present work were: **(i)**  $\Delta I / I_0$ , normalized current (at  $V_g = -$   
11  
12 20V); **(ii)**  $\Delta\mu_h / \mu_{h0}$ , normalized mobility; **(iii)**  $\Delta V_{th} / V_{th0}$ , normalized voltage threshold; **(iv)**  
13  
14  $\Delta I_{on/off} / I_{on/off0}$ , normalized on-off ratio of the current. Discrimination between the various VOCs  
15  
16 was achieved with the help of discriminant factor analysis (DFA). Statistical tests were  
17  
18 performed by SAS JMP, version 8.0. The program input consisted of various electronic features  
19  
20 from each sensor deduced from the exposure experiments.  
21  
22  
23  
24  
25  
26  
27

## 28 **RESULTS AND DISCUSSION**

29  
30 In the present study, we examined the advantages of using PAH-FET sensors to explore the  
31  
32 performance of the array in conjugation with pattern recognition methods.  
33  
34  
35  
36

### 37 ***Preliminary FET Device Characterization in Ambient Air***

38  
39 Figure 1a shows a schematic illustration of the PAH-FETs tested. Two sets of FETs were  
40  
41 prepared as described in the experimental section. The first set incorporated HTS-passivated field  
42  
43 oxide layers; the second set was fabricated using pristine oxide layers. Each of the two sets  
44  
45 included devices based on the seven PAH molecules shown in Figure 1b. The properties of the  
46  
47 molecules are listed in Table 1. Each device was fabricated in duplicate.  
48  
49  
50  
51  
52  
53  
54  
55  
56  
57  
58  
59  
60



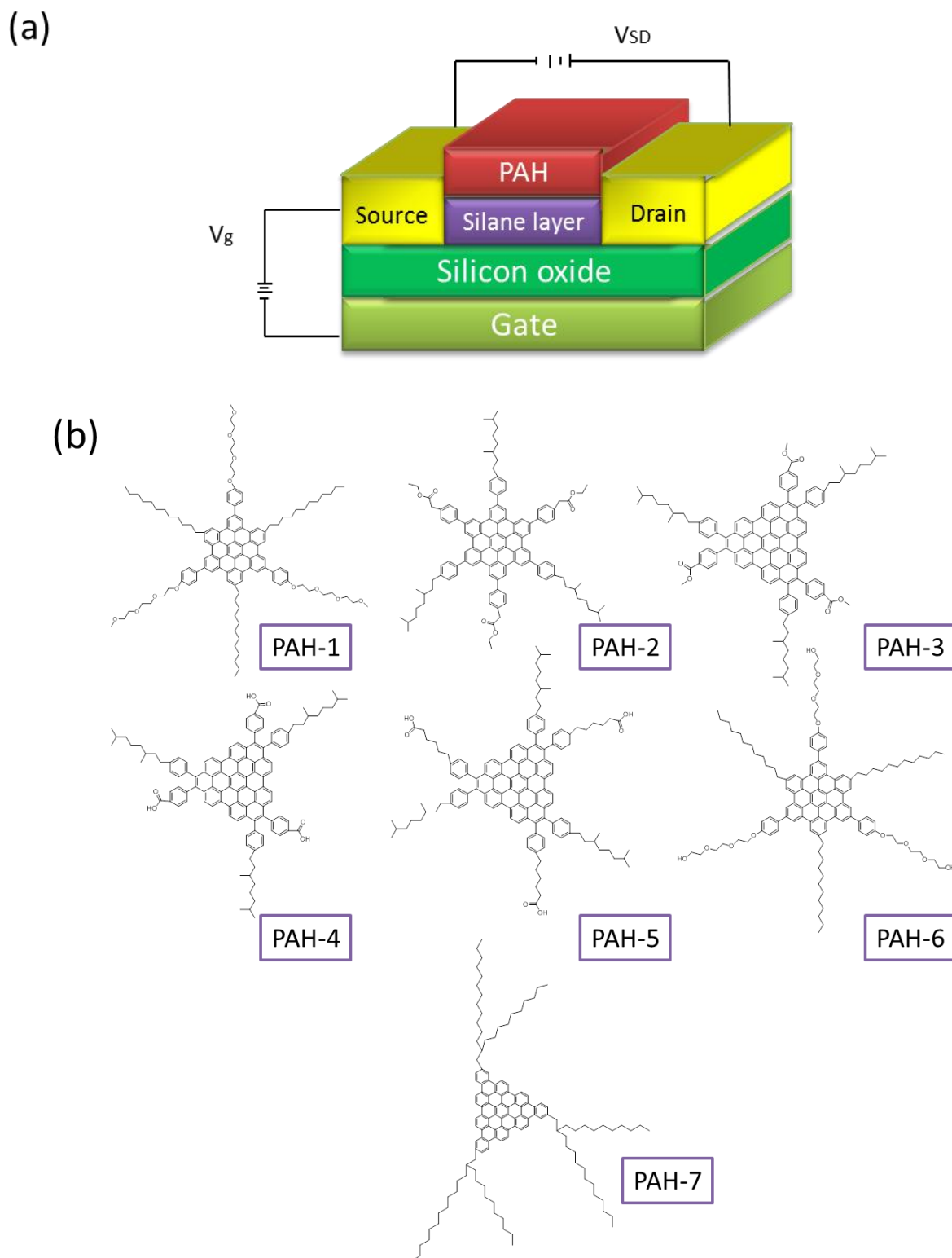
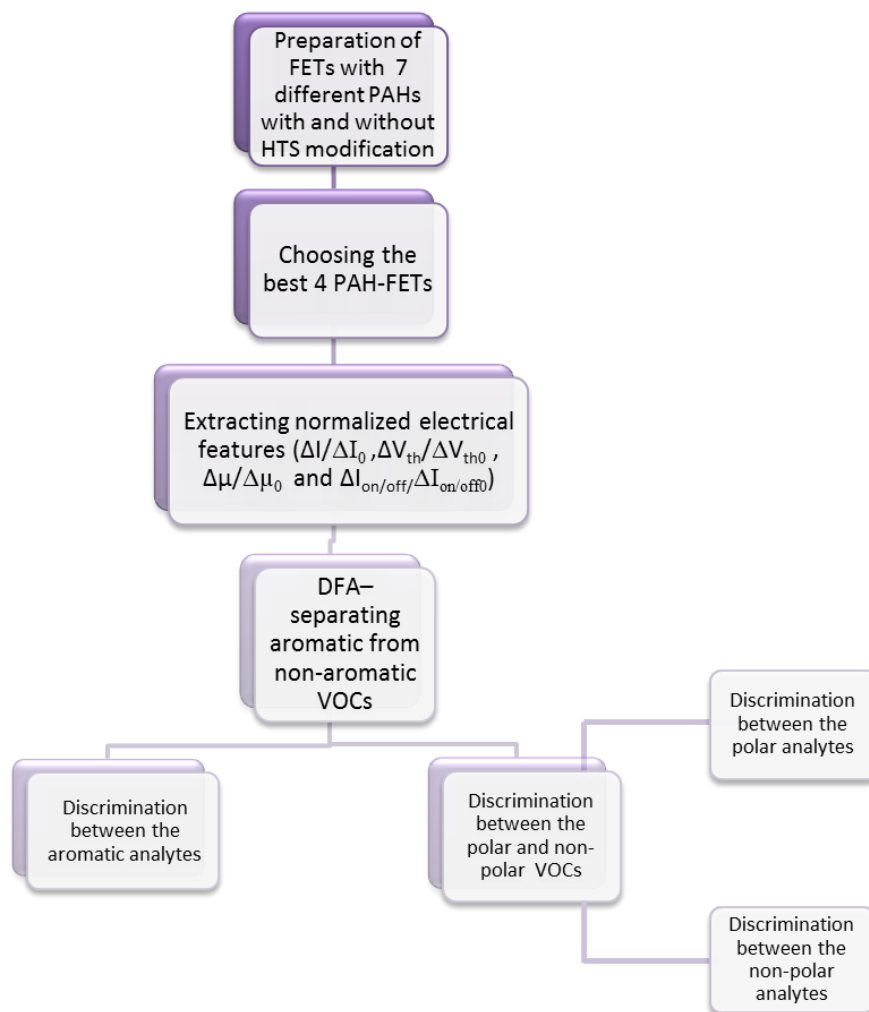


**Figure 1.** (a) Schematic representation of the sensor structure; and (b) Schematic drawing of the chemical structures of all PAHs tested in this study.

**Table 1.** Structural properties of all the PAH derivatives studied in the experiments

PAH derivative	Aromatic-core shape	No. of carbon atoms in the core	Side group	Side group polarity
PAH-1	Hexagonal	42	Ether	Weak polar
PAH-2	Hexagonal	42	Ester(ethyl)	Strong polar
PAH-3	Semi-triangular	48	Ester(methyl)	Strong polar
PAH-4	Semi- triangular	48	Carboxyl	Strong polar
PAH-5	Semi-triangular	48	Carboxyl	Strong polar
PAH-6	Hexagonal	42	Alcohol (hydroxyl)	Strong polar
PAH-7	Triangular	60	Alkyl chain	Non-polar

The outline of the work is represented by the flowchart in Figure 2. The first step was the choice of the most suitable PAH molecules for optimal FET performance. Measurements of  $I_{ds}$  vs.  $V_g$  in ambient air (RH ~ 40%), swept backward and forward between -40 V and 40 V at  $V_{ds} = 30$  V, showed that layers based on PAH-2,3,4&7 molecules yielded clearly superior devices than layers based on PAH-1,5&6. The signal-to-noise ratios for the former four molecules exceeded 13, whereas the latter three molecules yielded SNRs below 10. Furthermore, the average hysteresis between backward and forward back-voltage sweep (another important quality feature for FET sensors, which should be as small as possible, see below) was sufficiently small (<4V) for sensing applications in ambient atmosphere in devices based on PAH-1,5&6, but excessively large (>15V) for the devices based on PAH-1,5&6. In some of the measurements, the electrical features of PAH-1,5&6 could not even be extracted from the current vs. voltage curve, due to the lack of a clear field effect behavior. Consequently, we have performed the subsequent device characterization and the sensing experiments only on the devices based on PAH-2,3,4&7.

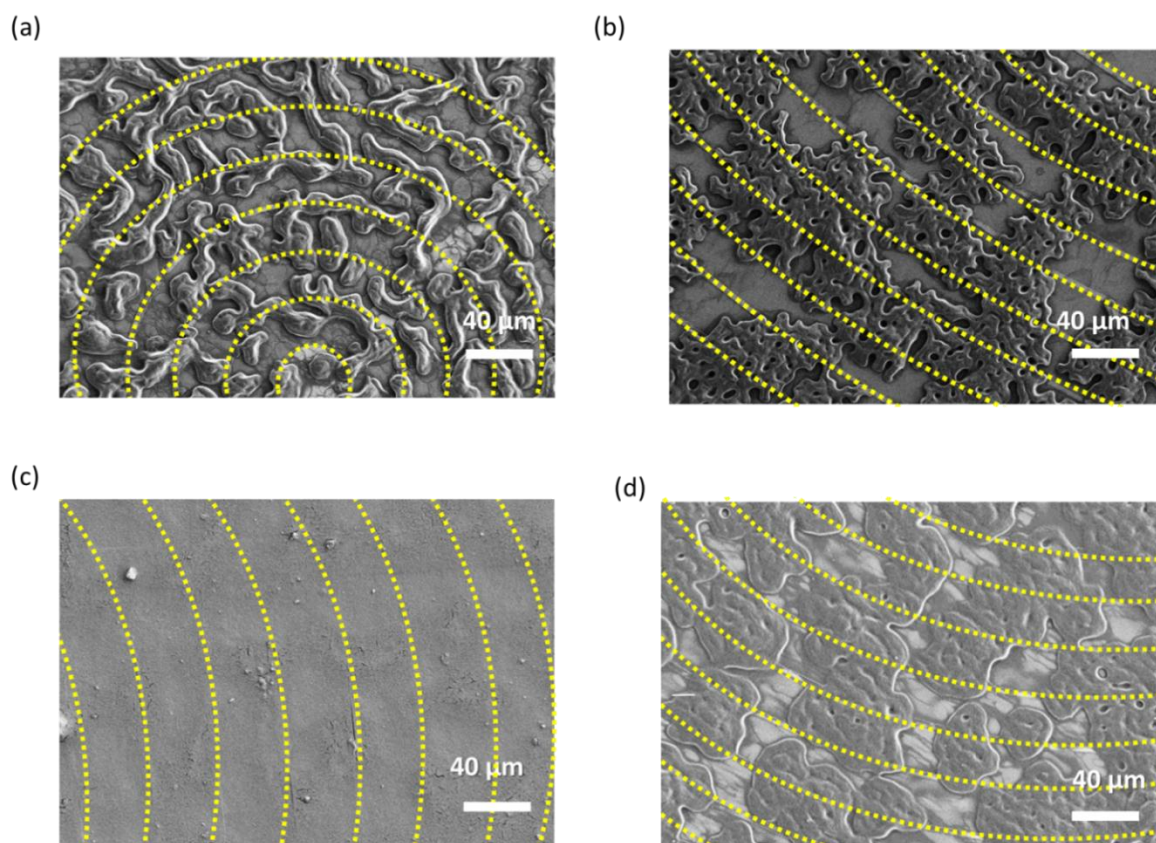


37 **Figure 2.** Flowchart representing the steps in analysis of the discriminative ability of the PAH FET array.  
38  
39

### 40 *Surface Morphology and Surface Coverage of the PAH-FETs*

41 **Figure 3** presents scanning electron microscopy (SEM) images of the PAH-2,3,4&7 layers  
42 covering the HTS-passivized FET devices. The corresponding devices on pristine oxide  
43 presented similar surface morphology and surface coverage for the different PAH molecules.  
44 Substantial differences in surface coverage and morphology were observed between the different  
45 molecules. Full surface coverage and smooth layers were obtained only for PAH-4 layers (*see*  
46 Figure 2c). PAH-2 has a surface coverage of  $57.4 \pm 15\%$  (*see* Figure 2a); PAH-3 has a surface  
47  
48  
49  
50  
51  
52  
53  
54  
55  
56  
57  
58  
59  
60

1  
2  
3 coverage of  $66.9\pm 11\%$  (see Figure 2b); and PAH-7 has a surface coverage of  $71.2\pm 5\%$  (see  
4  
5 Figure 2d). The incomplete coverage of the PAH-2, PAH-3, and PAH-7 films did not prevent  
6  
7 efficient electrical transport between the source and the drain, due to the formation of multiple  
8  
9 continuous PAH pathways between the adjacent islands and/or the source and drain electrodes.  
10  
11 The morphology of the various PAH films remained constant throughout the entire study. Neither  
12  
13 exposure to analytes nor humidity conditions changed the morphology of the PAH films (cf.  
14  
15 Figure 3 and Supporting Information, Figure S1).  
16  
17  
18  
19



48  
49  
50  
51  
52  
53  
54  
55  
56  
57  
58  
59  
60

**Figure 3.** Scanning electron microscopy images of FET surface that is covered with: (a) PAH-2 layer; (b) PAH-3 layer; (c) PAH-4 layer; and (d) PAH-7 layer, as prepared from  $10^{-3}$  M PAH solutions, before exposure to analytes. The positions of the 5  $\mu\text{m}$  wide interdigitated electrodes are highlighted by dashed yellow lines. The images were obtained with a secondary electron detector.

## The Effect of the Silane Layer on the Electronic FET Properties

The hysteresis that is typically observed between backward and forward back-voltage sweep forms one of the major obstacles to using FETs as gas sensors. The hysteresis is defined as the gap between the forward and backward electrical response in source-drain current while changing the back gate voltage.<sup>35</sup> The following explanation has been proposed: the silicon oxide ( $\text{SiO}_2$ ) surface allows the formation of surface trap states ( $\text{Si-OH}$ ,  $\text{Si-O}^-$ ,  $\text{Si-OH}^{2+}$  species)<sup>41</sup> that can function as sorption sites and, therefore, capture water molecules. When the relative humidity of the environment is high enough, water drops condensate on the  $\text{SiO}_2$  surface and is ionized. The resulting considerable changes in the FET characteristics are prone to mask the mild changes in the current induced by the targeted analyte(s).<sup>42</sup> **NOTE:** the  $\text{SiO}_2$  surface was extremely relevant to our case since PAH-2, PAH-3, and PAH-7 layers did not cover the entire oxide layer.

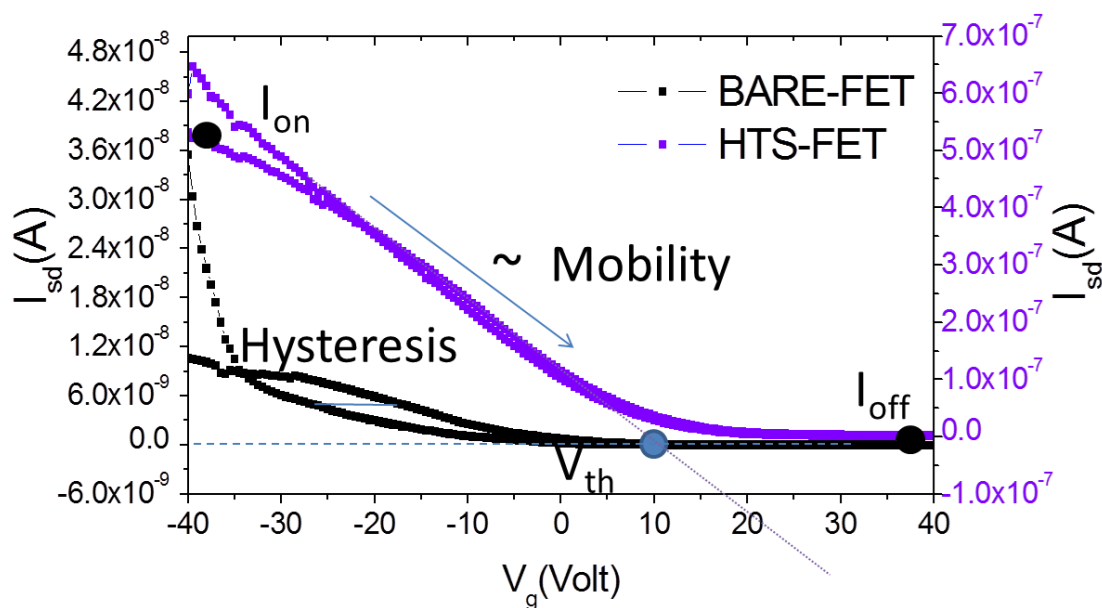


**Figure 4.** Linear characteristics of the source-drain current ( $I_{ds}$ ) vs. gate voltage ( $V_g$ ) of FET covered in PAH-2 layer with (purple curve) and without (black curve) HTS layer at the interface. The measurements were carried out by a forward and backward scan of  $V_g$  steps of 500mV, at  $V_{sd} = 30$  V.

Here we have investigated the feasibility of HTS surface modification as a way to remove the trap states from the SiO<sub>2</sub> surface, reducing the hysteresis effect. This approach has been proven as an efficient way to reduce the trap states (mainly Si–OH groups) on the SiO<sub>2</sub> surface, thus enhancing their related electrical and sensing features.<sup>33, 35</sup>

**Table 2.** Electrical features of the different PAH-FET devices, with and without the silane (HTS) surface modification.

	$I_{on}/I_{off}$		$V_{th}$ (V)		Hysteresis <sup>(a)</sup> (V)		Mobility (cm <sup>2</sup> V <sup>-1</sup> s <sup>-1</sup> )	
	Bare FET	HTS-FET	Bare FET	HTS-FET	Bare FET	HTS-FET	Bare FET	HTS-FET
PAH-2	223	381	-4.00	10.0	10.0	1.50	0.10E <sup>-6</sup>	0.36E <sup>-5</sup>
	±20.5%	±23.3%	±44.2%	±53.8%	±25.7%	±55.6%	±24.2%	±33.7%
PAH-3	1430	27300	-13.0	8.00	5.50	2.00	0.24E <sup>-6</sup>	0.14E <sup>-4</sup>
	±22.8%	±27.8%	±5.4%	±3.2%	±35.6%	±33.3%	±54.6%	±64.5%
PAH-4	134	281	7.00	8.00	12.0	3.00	0.13E <sup>-6</sup>	0.69E <sup>-6</sup>
	±33.5%	±26.6%	±17.1%	±14.3%	±22.4%	±16.7%	±10.7%	±5.7%
PAH-7	451	1930	-3.00	16.0	10.0	7.00	0.09E <sup>-6</sup>	0.50E <sup>-6</sup>
	±24.9%	±17.8%	±6.1%	±7.9%	±11.9%	±15.9%	±60.5%	±63.2%

<sup>(a)</sup> Hysteresis is represented by the largest distance (in the same current value) between the curves of the forward and backward current on the gate voltage axes.

It should be noted that only the SiO<sub>2</sub> was covered with the HTS molecules, but not the electrodes. Hence, the semiconducting PAH layers were in direct contact with the source and drain metal electrodes. Figure 4 and Table 2 show that the HTS surface modification improved almost all electrical features of the PAH-FETs studied. All examined devices exhibited higher current-on/current-off ( $I_{on}/I_{off}$ ) ratio, indicating an improvement in the electrical efficiency of the FET device. Note, however, that higher values of  $I_{on}/I_{off}$  do not necessarily imply enhancement in

1  
2  
3 *the sensitivity and selectivity for sensing applications.* All PAH-FET devices examined exhibited  
4 elevated values of carrier mobility, indicating an improvement in the conductivity of the charge  
5 carrier tunnel. FETs that were covered with *discontinuous* layers of PAH-2, PAH-3 or PAH-7  
6 exhibited negative  $V_{th}$  without the HTS modification and positive  $V_{th}$  with the HTS modification,  
7 meaning that the p-type device (that usually conducts current in the negative values of gate  
8 voltage) is open over a wider range of voltages. On the other hand, the FETs that were covered  
9 with continuous layers of PAH-4 exhibited positive  $V_{th}$  without the HTS modification and  
10 negative  $V_{th}$  with the HTS modification. In this device, the HTS seems to increase of the  
11 resistance between the gate and the semiconducting PAH-4 layer. Of great importance, the  
12 addition of the HTS modification has shown a clear effect on the hysteresis of the examined  
13 devices, in the following order: PAH-2 < PAH-4 < PAH-3 < PAH-7. PAH-2 with HTS  
14 modification has shown the smallest hysteresis and, hence, is the least sensitive to water.  
15  
16  
17  
18  
19  
20  
21  
22  
23  
24  
25  
26  
27  
28  
29  
30  
31  
32  
33

### 34 ***Sensing of VOCs with PAH-FETs***

35  
36 FETs covered with PAH-2, PAH-3, PAH-4 and PAH-7 layers were exposed to several  
37 representative analytes from three chemical groups (alcohols, alkanes and aromatic compounds).  
38 The analytes and their physical and chemical properties are listed in Table 3. The gate voltage  
39 ( $V_g$ ) was swept from -40 V to +40 V at  $V_{ds} = 30$  V. The following features were extracted: (i)  $I$  at  
40  $V_g = -20$  V, the current value at gate voltage of -20V; (ii)  $\mu_h$ , hole mobility values extracted from  
41 the  $I_{ds}$  vs.  $V_g$  curve, using the following equation:  
42  
43  
44  
45  
46  
47  
48  
49  
50  
51  
52

$$53 \mu_h = \frac{L}{ZC_i} \frac{1}{V_{ds}} \frac{\partial I}{\partial V_g} \quad (1)$$

54  
55  
56  
57  
58  
59  
60

1  
2  
3 where  $L$  is the length of conductive channel,  $Z$  is the width of the conductive channel,  $V_{ds}$  is the  
4  
5 voltage applied between the source and drain electrode,  $C_i$  is the capacitance per unit area of the  
6  
7 silicon oxide layer,  $I$  is the current, and  $V_g$  is the voltage applied on the gate electrode; (iii)  $V_{th}$ ,  
8  
9 voltage threshold calculated by extrapolating the linear part of the  $I_{ds}$  vs.  $V_g$  curve and extracting  
10  
11 the interception value with the voltage axis (see Figure 4); (iv)  $I_{on/off}$ , the ratio between the  
12  
13 current-on ( $I_{on}$ ), and current-off ( $I_{off}$ ), calculated by dividing the current value when the device is  
14  
15 "open" (i.e.,  $I_{on}$ ) – an average of five measurements of current ending with  $V_g = -40V$  – by the  
16  
17 value when the device is "closed" (i.e.,  $I_{off}$ ) – an average of five measurements of current starting  
18  
19 with  $V_g = +40V$ . For the final analysis, normalized values of each feature were obtained by  
20  
21 dividing the sensor's steady state feature under analyte exposure by the baseline value. According  
22  
23 to the following equation:  
24  
25  
26  
27  
28

$$29 \quad \text{normalized feature} = \frac{\Delta r}{r_0} = \frac{r_1 - r_0}{r_0} \quad (2)$$

30  
31  
32 where  $r_0$  is an average of five measurements at the end of the air exposure step, and  $r_1$  is an  
33  
34 average of five measurements at the end of an analyte exposure step. A representative example of  
35  
36 the normalized sensing feature ( $\Delta r/r_0$ ) as a function of time is presented and discussed in Figure  
37  
38  
39  
40  
41  
42  
43  
44  
45  
46  
47  
48  
49  
50  
51  
52  
53  
54  
55  
56  
57  
58  
59  
60  
S2 of the supporting information.



**Table 3.** Physical and chemical properties of the VOCs used as analytes for the exposure experiments

VOC	Formula	$p_o$ (kPa @ 20°C) <sup>(a)</sup>	Dipole Moment (Debye)	Density (g·cm <sup>-3</sup> )	Molecular weight (gr·mol <sup>-1</sup> )
Hexane	CH <sub>3</sub> (CH <sub>2</sub> ) <sub>4</sub> CH <sub>3</sub>	17.6	0	0.655	86.2
Octane	CH <sub>3</sub> (CH <sub>2</sub> ) <sub>6</sub> CH <sub>3</sub>	1.47	0	0.703	114
Decane	CH <sub>3</sub> (CH <sub>2</sub> ) <sub>8</sub> CH <sub>3</sub>	1.58	0	0.730	142.2
Octanol	CH <sub>3</sub> (CH <sub>2</sub> ) <sub>7</sub> OH	0.114	2.00	0.824	130
Decanol	CH <sub>3</sub> (CH <sub>2</sub> ) <sub>9</sub> OH	0.0148	1.68	0.830	158.3
Mesitylene	C <sub>6</sub> H <sub>3</sub> (CH <sub>3</sub> ) <sub>3</sub>	0.230	0	0.864	120
Styrene	C <sub>6</sub> H <sub>5</sub> CH=CH <sub>2</sub>	0.670	0.130	0.909	104
Ethylbenzene	C <sub>6</sub> H <sub>5</sub> -C <sub>2</sub> H <sub>5</sub>	0.900	0.240	0.867	106
Toluene	C <sub>6</sub> H <sub>5</sub> -CH <sub>3</sub>	3.80	0.360	0.866	92.1

<sup>(a)</sup>  $p_o$  stands for the VOC's vapor pressure at 20 °C.<sup>43</sup>

Figures 5a & 5b show the normalized current,  $\Delta I / I_0$ , under exposure to different analytes in 5% RH environment. Most responses are negative. Certain trends were identified, for example, the responses of PAH-2 & 3 (5% RH) to the aromatic analytes scaled with the analytes' polarity: the higher the polarity of the analyte, the greater the decrease in normalized current. In general we can see that the absolute responses of all four sensors to the exposure with aromatic VOCs were higher than to the exposure with non-aromatic VOCs. By comparing the normalized current responses obtained under 5% and 40% RH (*see* Figures 5a & 5c), we found that the effect of the humidity background was considerable on the FETs based on PAH-3 and PAH-4: neither the values, the direction of the change, nor the trend of the response were similar between the changing environments. For FETs based on PAH-2 and PAH-7 films, the changes were less

drastic: the responses on exposure to VOCs fewer than 5% RH were slightly diminished when the humidity of the background increased to 40% RH, but the general trends were not changed.

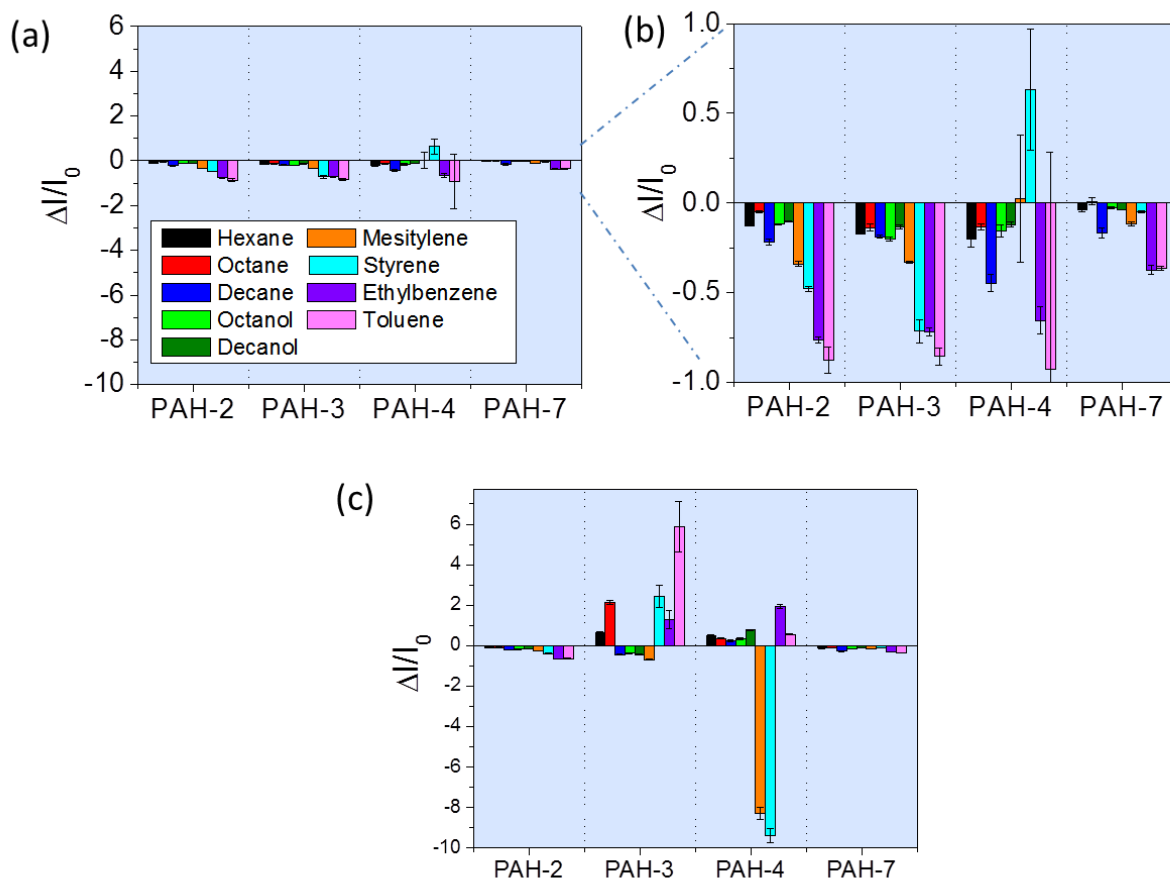


**Figure 5.** Normalized current (at  $V_g = -20V$ ) ( $\Delta I / I_0$ ) while exposing the devices to different analytes in a concentration of  $p_a/p_o=0.1$  in an environment of (a) 5% RH; (b) 5% RH (magnification); and (c) 40% RH. Each value is the average of two repeated exposures in the same conditions.

Figure 6 presents the normalized mobility,  $\Delta\mu_h / \mu_{h0}$ , of the sensors under VOC exposure. Most of the exposures resulted in a decrease in normalized mobility. PAH-2 and PAH-3 exhibited only a decrease in mobility in both low (5%) and high (40%) relative humidity (RH) environments. On the other hand, PAH-4 and PAH-7 showed both increase and decrease,

1  
2  
3 depending on the types of the exposed VOC and RH level. Another noticeable fact is that PAH-2  
4  
5 and PAH-3 displayed lower standard deviations, compared with the PAH-4 and PAH-7. PAH-2  
6  
7 and PAH-3 discriminated well between the various VOCs based on the normalized mobility  
8  
9 feature alone. *PAH-2 is of special interest since the discrimination ability of this device was not*  
10  
11 *(or minimally) affected by the RH level of the exposure environment.* Indeed, neither the  
12  
13 response magnitude nor the ratio between the responses obtained on exposure to various VOCs  
14  
15 was affected. In the category of aromatic VOCs exposed to PAH-2&3, a disproportional  
16  
17 relationship was found between the normalized mobility response (mesitylene < toluene < styrene  
18  
19 <ethylbenzene) and the VOC polarity, both at low and high RH levels (*see* Figures 6a and 6b):  
20  
21 the higher the polarity, the lower the normalized mobility value. An exception was the response  
22  
23 of PAH-2 to toluene. It is likely that the toluene adsorbed quite strongly to the PAH-2 surface,  
24  
25 leaving significant residues within the sensing film during the cleaning process with dry air. The  
26  
27 substantial decrease in normalized mobility on exposure to aromatic VOCs could be related to  
28  
29 one or both of the following reasons: **(i)** the aromatic VOCs have higher bonding strength to the  
30  
31 surface, having greater effect on the charge carrier's mobility, perhaps due to swelling of the  
32  
33 PAH layers; **(ii)** the higher absorption ability of aromatic VOCs causes a greater dipole-induced  
34  
35 field than the other groups of VOCs (alcohols and alkanes), interfering with the field caused by  
36  
37 the gate electrode. No relationship was found between the normalized mobility response and the  
38  
39 polarity of non-aromatic VOCs.  
40  
41  
42  
43  
44  
45  
46  
47  
48  
49  
50  
51  
52  
53  
54  
55  
56  
57  
58  
59  
60

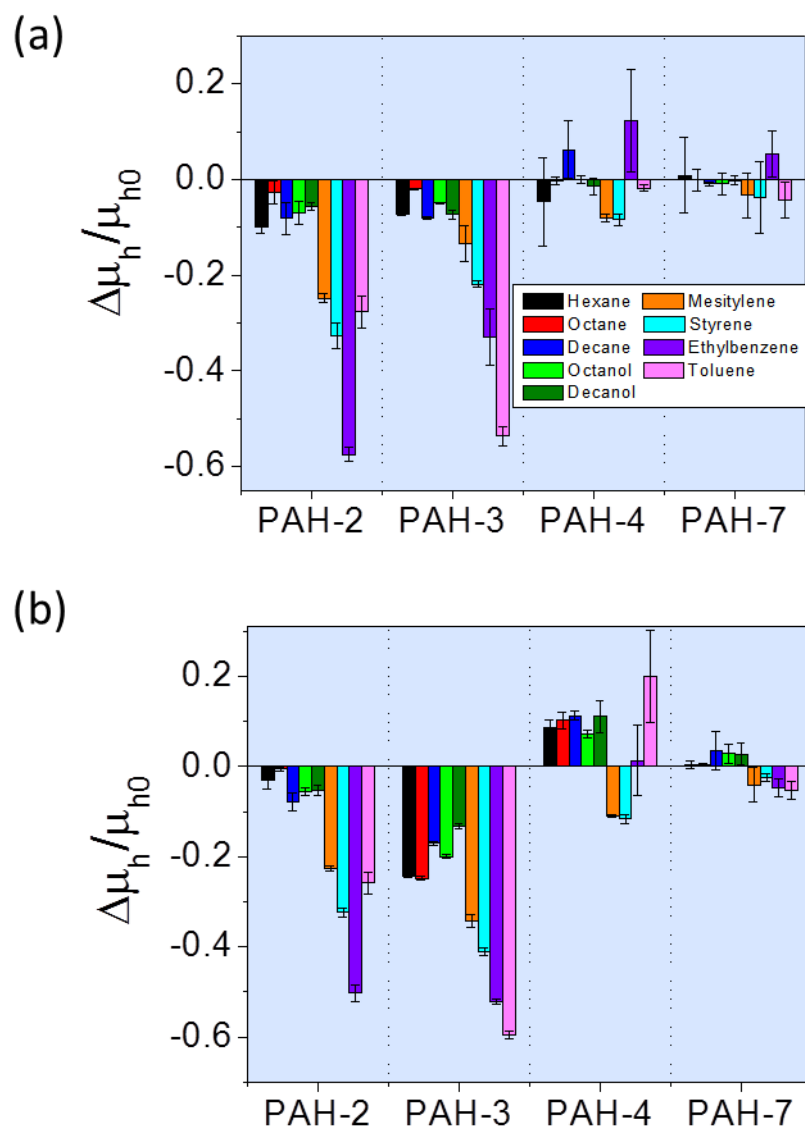


**Figure 6.** Normalized mobility values while exposing the devices studied to different analytes in an environment of (a) 5% RH; and (b) 40% RH. The concentration in both figures is  $p_d/p_o=0.1$ . Each value is the average of two repeated exposures in the same conditions.

PAH-3 and PAH-4 have the same aromatic core (semi-triangle) and organic side chains, but slightly differ in the termination groups of the organic side chains (ester group in PAH-3 and carboxylic group in PAH-4). Integrating PAH-3 and PAH-4 in FET platforms exhibited

1  
2  
3 substantially different normalized mobility responses on exposure to the same conditions. This  
4  
5 observation stresses the importance of the PAH's side chain for sensing applications. Side chains  
6  
7 mediate the interaction between the VOC and the charge carrier channel of the organic  
8  
9 semiconductor. They also play an important role in the self-assembly and morphology of the  
10  
11 PAH on the surface – another reason for the discrepancies in the sensing characteristics of the  
12  
13 sensors. The PAH-7 sensor exhibited responses at the order of, or lower than, the experimental  
14  
15 variance(s) of the sensing measurements. Therefore, no clear relationship between the normalized  
16  
17 mobility responses and VOC characteristics could be established. Looking at **Figures 5&6**, we  
18  
19 see that each feature of each sensor has distinctive individual behavior as a result of the exposure,  
20  
21 varying from analyte to analyte and also changing with the humidity levels. These variations of  
22  
23 features and sensors give us the variability we need in the array of sensors as a whole, to  
24  
25 discriminate between different analytes.  
26  
27  
28  
29  
30

31 **Figure7** shows the effect of analyte exposure in different background humidity on the  
32  
33 normalized threshold voltage,  $\Delta V_{th} / V_{th0}$ . PAH-2 exhibited the highest variability of response,  
34  
35 both in high and low humidity: the responses to toluene and ethyl benzene (two of the most polar  
36  
37 analytes) were one order of magnitude higher than to the remaining analytes. The values of  
38  
39 normalized  $V_{th}$  were positive in dry conditions. However, under 40% RH, PAH-4 showed  
40  
41 negative responses to some analytes. No substantial other trends were noticed, but we can  
42  
43 conclude that the feature is very sensitive to humidity changes in the environment.  
44  
45  
46  
47  
48  
49  
50  
51  
52  
53  
54  
55  
56  
57  
58  
59  
60

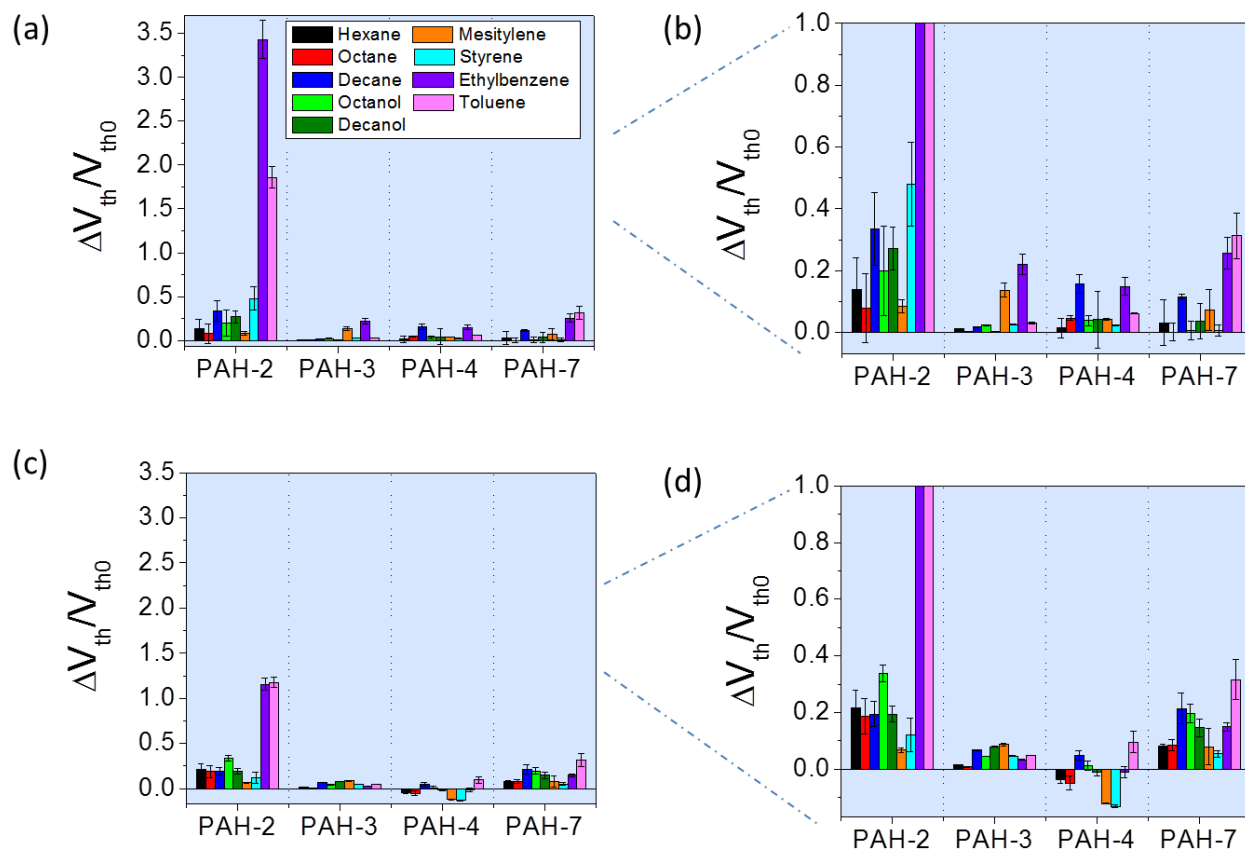


**Figure 7.** Normalized threshold voltage during exposure to different analytes in an environment of (a) 5% RH; and (c) 40% RH. (b) & (d) are the magnifications of (a) & (c). The concentration in both figures is  $p_d/p_o = 0.1$ . Each value is the average two repeated exposures in the same conditions.

Figure 8 presents the normalized ratio between the averaged current when the channel is open ( $I_{on}$ ) and closed ( $I_{off}$ ). As seen in the figure, the experimental error is usually higher than the response value *per se*. These results imply that  $\Delta I_{on/off} / I_{on/off0}$  cannot serve as a sensing feature, at either low or at high RH levels. Therefore, the feature was not included in the DFA analysis. As previously seen in Figure S2(d) of the supporting information, the response of the feature (even before normalization) does not give any reliable information. These high variances are

caused by the inconsistent and noisy values for the off-current-ranging from  $1E^{-13}$  to  $8E^{-11}$  A, the low values of the off current are difficult to measure in the system used. In future exposure experiments we can try to measure with a more sensitive system, or this noisy feature can be replaced by the on-current value.

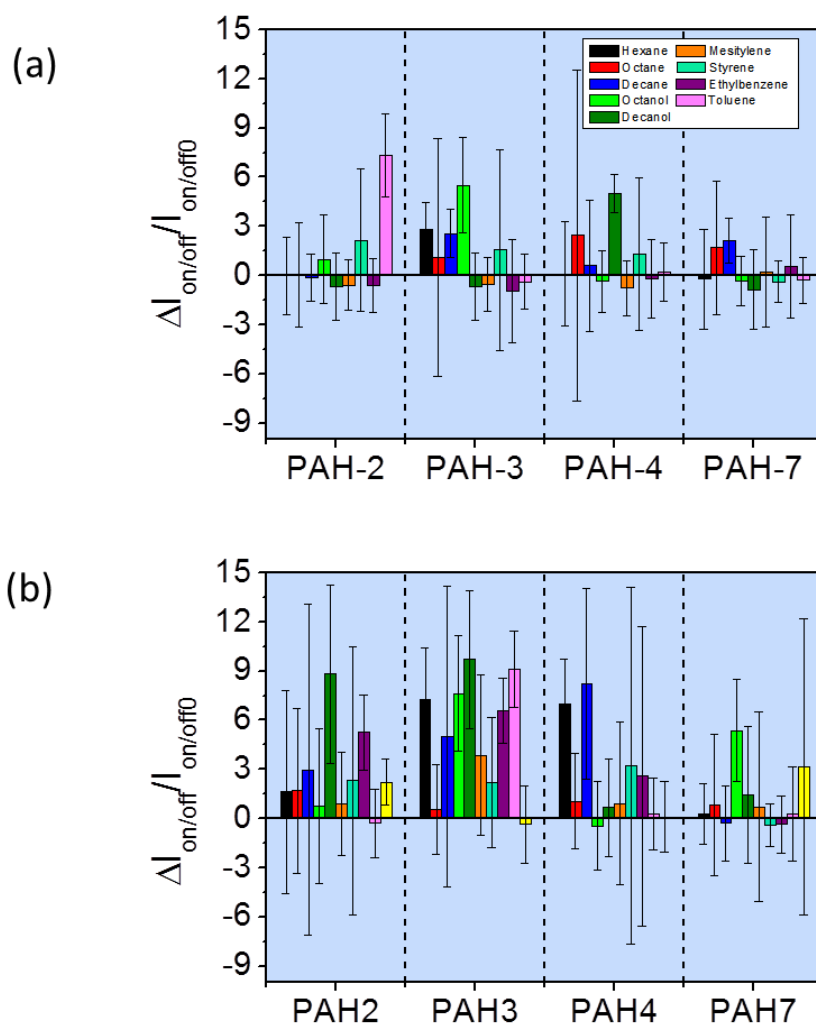


**Figure 8.** Normalized ratio between the averaged current when the device is open ( $I_{on}$ ) and the value when the device is closed ( $I_{off}$ ). The values calculated from the different sensors while exposing the device to different analytes in an environment of (a) 5% RH; and (b) 40% RH. Each value is the average of two repeated exposures in the same conditions.

### VOC Sensing using Patterns from Combinations of Sensing Features

Discriminant factor analysis (DFA) was employed for effectively discriminating between: (i) aromatic and non-aromatic VOCs; (ii) polar and non-polar analytes; (iii) the studied VOCs in each sub-group, as shown in Figure 2. To evaluate the accuracy of differentiation, we also investigated other combinations of normalized features (of equal number) and estimated their accuracies according to the leave-one-out method.

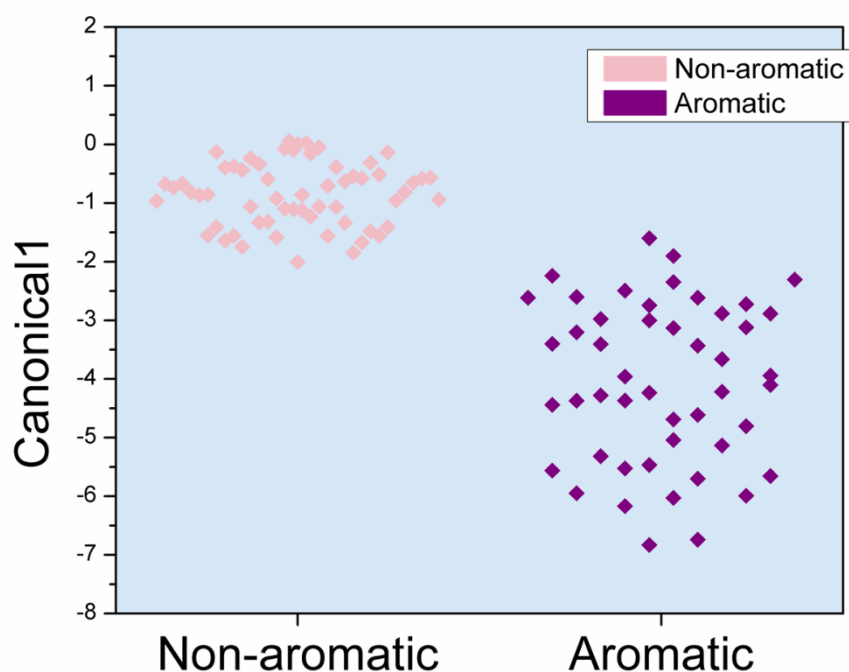


**Figure 9.** DFA results separating the non-aromatic (octanol, decanol, hexane, octane, decane) and aromatic VOCs (mesitylene, styrene, ethyl-benzene, toluene) at different concentrations ( $p_a/p_o=0.05, 0.1, 0.2$ ), both in 5% and in 40% RH. Each value is the average of two repeated exposures in the same conditions.



1  
2  
3 Figure 9 presents a DFA map separating between aromatic and non-aromatic VOC  
4 groups. A high separation accuracy (using the leave-one-out method) of 95.37% was achieved,  
5 using only one variable, namely  $\Delta\mu_h / \mu_{h0}$  of the PAH-2 sensor. A single sensor provided us with  
6 a highly accurate separation, despite the fact that the VOCs were tested in different humidity  
7 conditions and at different concentrations. The fact that the separation is based on PAH-2  
8 matches the conclusions seen from Table 3, which shows that PAH-2 is least sensitive to  
9 water/humidity. Hence, PAH-2 made it possible to separate between VOCs according to their  
10 chemical or physical properties, irrespective of the confounding humidity. Table S3 of the  
11 Supporting Information illustrates the advantage of PAH-2 over the other sensors: PAH-2 gives  
12 the highest accuracy of separation compared to the features from other sensors. The choice of the  
13 normalized mobility is also not coincidental, because the normalized mobility of PAH-2 gives  
14 significantly different values when exposed to aromatic analytes compared to non-aromatic ones  
15 and is less affected by changes in the humidity (*see* Figure 6). Additionally, the aromatic cluster  
16 is less well defined than the cluster of the non-aromatic analytes (*see* Figure 9). Using only one  
17 sensor is of great significance for future applications, ensuring easy device fabrication and use as  
18 well as simple analysis.  
19  
20  
21  
22  
23  
24  
25  
26  
27  
28  
29  
30  
31  
32  
33  
34  
35  
36  
37  
38  
39  
40  
41  
42  
43  
44  
45  
46  
47  
48  
49  
50  
51  
52  
53  
54  
55  
56  
57  
58  
59  
60

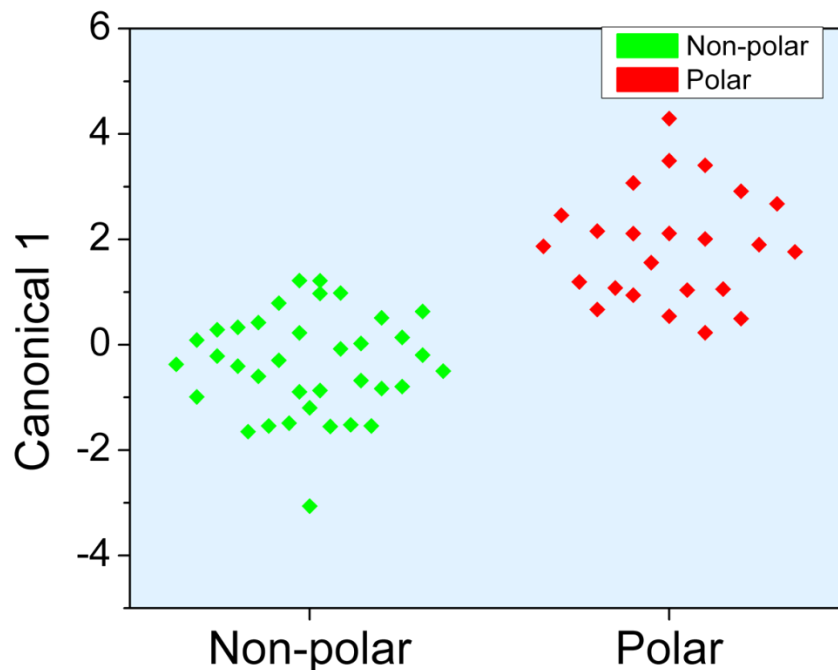


**Figure 10.** DFA results separating the polar material (octanol, decanol) from the non-polar (hexane, octane, decane) at different concentrations ( $p_a/p_o=0.05, 0.1, 0.2$ ), both in 5% and in 40% RH. Each value is the average of two repeated exposures in the same conditions.

Next, we distinguished the polar and non-polar non-aromatic compounds. The results are represented in Figure 10. We used different combinations of three features from four PAH-FETs:  $\Delta I / I_0$  of PAH-2,3,4&7,  $\Delta\mu_h / \mu_{h0}$  of PAH-4&7 and  $\Delta V_{th} / V_{th0}$  of PAH-3&7. The accuracy of separation received by the leave-one-out method is 80%.

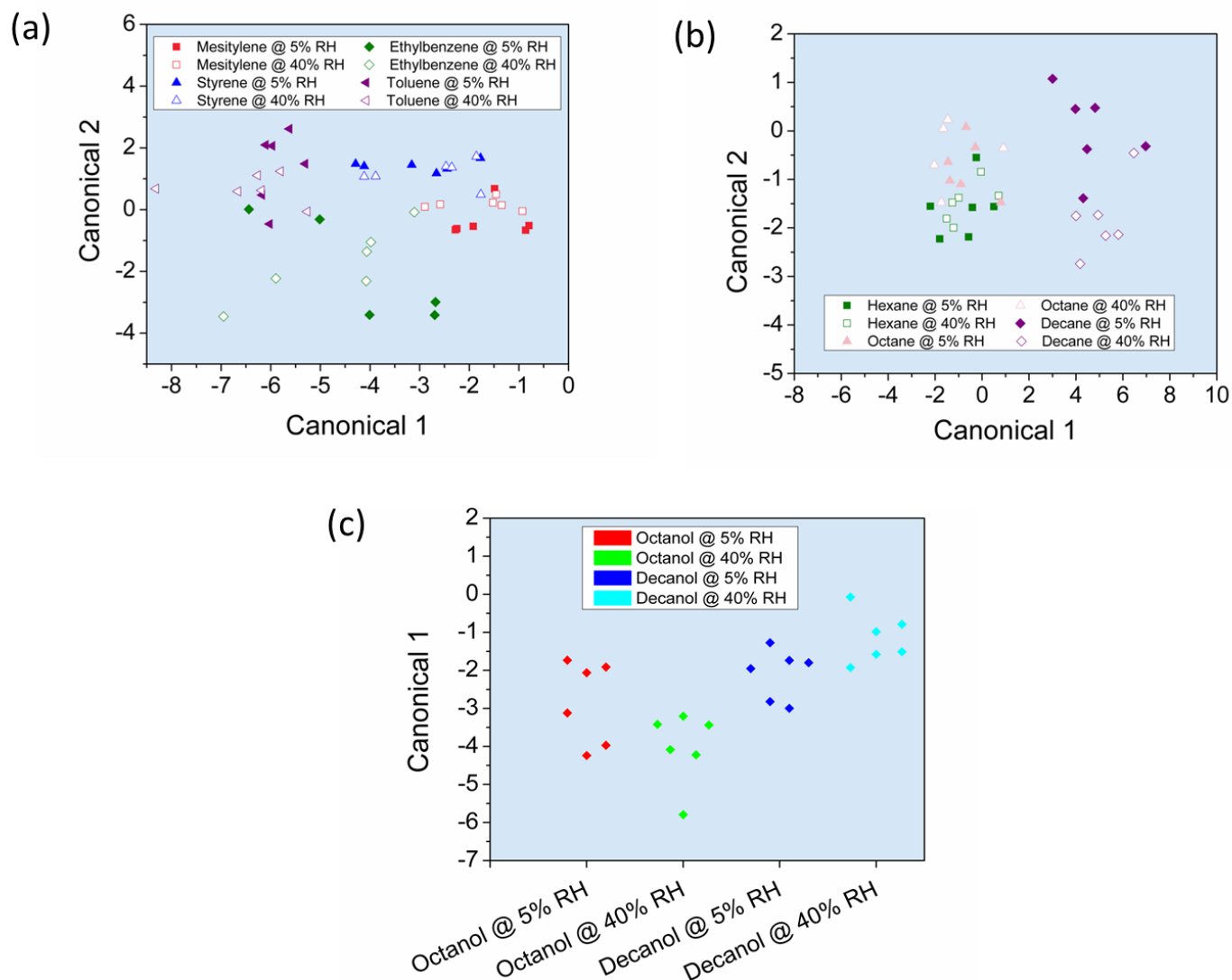


**Figure 11.** DFA results separating: (a) aromatic material (mesitylene, styrene, ethyl-benzene, toluene); (b) non-polar VOCs (hexane, octane, decane); (c) polar materials (octanol, decanol). The various dots stand for the response of the device on exposure to different concentrations ( $p_a/p_o=0.05, 0.1, 0.2$ ) of the different VOCs in both 5% and 40% RH. Each value is the average of two repeated exposures in the same conditions.

1  
2  
3 The separation between polar and non-polar non-aromatic compounds was less accurate  
4 than the separation between aromatic and non-aromatic compounds. Other combinations of  
5 sensing features provided even lower accuracy (*see Supporting Information, Table S4*). Using  
6 a combinations of all sensors and all features provided better results than using either the features  
7 from one separate sensor (*see Supporting Information, Table S4(b)*) or some of the sensors  
8 (*see Supporting Information, Table S4(a)*).

9  
10  
11  
12  
13  
14  
15  
16  
17  
18 After separating the polar and non-polar non-aromatic compounds, we tested the array's  
19 ability to differentiate between the specific VOCs in each group. In the aromatic group (*see*  
20 Figure 11a) the separation is based on 8 parameters:  $\Delta I / I_0$  of PAH-2&7,  $\Delta V_{th} / V_{th0}$  of PAH-2&7  
21 and  $\Delta \mu_h / \mu_{h0}$  of PAH-2,3,4&7. The resulting accuracy was 75%. Again, all the sensors and all  
22 the features were needed for the separation. It is reasonable to assume that the high absorbance of  
23 the aromatic VOCs makes them easy to discriminate from the other VOCs. However, identifying  
24 the separate aromatic VOCs would be more difficult. Figure 11a shows that the analytes were  
25 mostly separated along the negative axis of the first canonical variable, according to their polarity  
26 (except for ethyl benzene). The least polar analyte, mesitylene, has the least negative CV1 values;  
27 toluene, the most polar analyte, has the most negative CV1 value. No clear separation is seen  
28 between the 5%RH and the 40%RH of the same analyte, perhaps being an indication that the  
29 separation is less sensitive to humidity changes. Table S5 of the Supporting Information shows  
30 that a combination of all features from all sensors provides the highest accuracy of  
31 discrimination.

32  
33  
34  
35  
36  
37  
38  
39  
40  
41  
42  
43  
44  
45  
46  
47  
48  
49  
50  
51  
52  
53  
54  
55  
56  
57  
58  
59  
60  
Figure 11b shows the separation between the different VOCs in the non-polar group  
(hexane, octane and decane). The accuracy obtained was 75% and was based on 6 parameters ( $\Delta I / I_0$  of PAH-3&7,  $\Delta V_{th} / V_{th0}$  of PAH-3&7, and  $\Delta \mu_h / \mu_{h0}$  of PAH-3&4). Decane was separated

1  
2  
3 from the rest of the analytes along the axis of the first canonical variable alone, while hexane and  
4  
5 octane were separated along the axis of the second canonical variable. As before, no significant  
6  
7 difference could be noticed between the 5% RH and the 40% RH. The combination that gave the  
8  
9 best separation did contain features from the PAH-2 sensor, but included all four types of features  
10  
11 to receive an accuracy of 75%. The same accuracy was achieved by using all the sensors in the  
12  
13 combinations presented in the Supporting Information, Table S6(a). By including more features  
14  
15 in the analysis we can reduce, in this case, the number of sensors in the array and still achieve the  
16  
17 same accuracy. When comparing the accuracy of the combination used in **Table S6(c) of the**  
18  
19 **Supporting Information** to the accuracy in the separation chosen for nonpolar VOCs, we  
20  
21 observed that better results could be achieved by using less sensors but extracting more features  
22  
23 per sensor.  
24  
25  
26  
27  
28

29  
30 Previously, the same PAH molecules were utilized in chemiresistors<sup>27</sup> which could  
31  
32 provide only one independent sensing feature. Using chemiresistors based on three types of  
33  
34 PAHs, the same VOCs at similar concentrations (varying from  $p_d/p_o=0.04$  and up to  $p_d/p_o=1$ )  
35  
36 could be distinguished with an accuracy of 71%. In the present work, an array of three PAH-  
37  
38 FETs based on PAH-3,4&7 yielded higher separation accuracy (75%). It should be noted that the  
39  
40 highest concentration we used was  $p_d/p_o=0.2$ , while in previous studies it was  $p_d/p_o=1$  (the higher  
41  
42 the concentration, the easier it is to separate the different analytes). Since FET arrays allow  
43  
44 extracting more independent features per sensor, their discriminative power is superior, while  
45  
46 using the same number or fewer sensors. Instead of including another kind of device to improve  
47  
48 the sensing abilities of the array, we can exploit another feature of the same sensor for improved  
49  
50 sensing.  
51  
52  
53  
54  
55  
56  
57  
58  
59  
60

1  
2  
3 Figure 11c shows the separation of the polar group (between octanol and decanol);  
4  
5 analysis is based on 4 parameters:  $\Delta I / I_0$  of PAH-3&4 and  $\Delta\mu_h / \mu_{h0}$  of PAH-2&3; the accuracy  
6  
7 of separation 79%. The two analytes were separated along the canonical-1 axis. In contrast to  
8  
9 sensing non-polar VOCs (using PAH-3,4&7), sensing the polar VOC analysis required  
10  
11 substituting the PAH-7 sensor (non-polar-aliphatic side group) with the PAH-2 sensor (polar –  
12  
13 ester side group). This indicates that controlling the side groups controls the adsorption of the  
14  
15 VOCs, thus affecting the sensing abilities. The PAH-FET array was more sensitive to polar  
16  
17 analytes (79% accuracy of separation) than non-polar ones (75% accuracy of separation). This  
18  
19 was possibly due to screening against the absorption of the non-polar analytes by the mostly  
20  
21 polar side groups of the PAH molecules.  
22  
23  
24  
25  
26

27 When analyzing the sensing abilities of the PAH-FET array, it is important to clarify that  
28  
29 the different responses of the sensors are due to the chemistry of the organic semiconductor rather  
30  
31 than the surface coverage. It was previously reported that the signals of the sensors to different  
32  
33 analytes can be controlled by changing the surface coverage of the sensing material. Hence, a  
34  
35 sensor array based on layers of the same PAH molecule, but with different surface coverage,  
36  
37 could be created.<sup>29</sup> The surface coverage of our sensors is in the following order: PAH-4 > PAH-  
38  
39 7 > PAH-3 > PAH-2. The accuracy of separation of each sensor was calculated with the leave-  
40  
41 one-out method by choosing all three features from each sensor and basing the discrimination on  
42  
43 it alone. The order of accuracy when trying to separate, for example, the polar analytes from the  
44  
45 non-polar is PAH-3&4 > PAH-2 > PAH-7, meaning PAH-3&4 gave the most accurate  
46  
47 separation. When trying to separate the aromatic analytes, the accuracy achieved was in the  
48  
49 following order: PAH-7 > PAH-3 > PAH-2 > PAH-4. Comparing the orders of accuracy shows  
50  
51 that there is no correlation between the surface coverage and the sensing abilities of the sensors.  
52  
53  
54  
55  
56  
57  
58  
59  
60

1  
2  
3 Furthermore, it is incorrect to declare a certain sensor to have greater sensing abilities that  
4 another, since the sensitivity of each device changes as a result of the separation required. An  
5 array's separation capability is based on the properties of the sensing layer and the analytes and  
6 the mechanism applied between the two factors.  
7  
8  
9  
10  
11

## 12 13 14 15 **SUMMARY AND CONCLUSIONS**

16  
17 We have demonstrated the feasibility of PAH-FET sensors for VOC sensing applications in  
18 humid atmospheres. The ability to extract multiple electrical features as well as multiple signal  
19 features from each PAH-FET sensor provided a reservoir of sensing signals that allowed  
20 discrimination between aromatic and non-aromatic VOCs, discrimination between polar and non-  
21 polar non-aromatic compounds, and identification of specific VOCs within the sub-groups (*i.e.*  
22 aromatic compounds, polar non-aromatic compounds, non-polar non-aromatic compounds) at  
23 both low and high RH levels. So far, the multiplicity of features extracted from PAH-FET  
24 sensors provide superior performances than similar PAH materials that are integrated within  
25 chemiresistive platforms (or FET at  $V_g = 0$ ). In a few cases, one could expect that a single PAH-  
26 FET sensor would demonstrate a similar performance to an array of chemiresistive sensors that  
27 are based on the same PAH layer. This result is of great importance for the construction of  
28 miniaturized, self-learning sensing systems that can work independently under real, confounding  
29 factors. Using the PAH-FET sensors, it would be possible to exchange information and construct  
30 a miniaturized model of some environmental properties under observation. Such a model could  
31 then be used to classify events of interest and take action on the basis of a high-level  
32 representation of the system context. This would allow large-scale information and  
33 communication systems using the model to autonomously adapt to highly dynamic and open  
34 environments. Ultimately, the results presented here could lead to the development of cost-  
35  
36  
37  
38  
39  
40  
41  
42  
43  
44  
45  
46  
47  
48  
49  
50  
51  
52  
53  
54  
55  
56  
57  
58  
59  
60

1  
2  
3 effective, lightweight, low-power, non-invasive tools for the widespread detection of VOCs in  
4  
5 real-world applications, including, but not confined to environmental, security, food industry,  
6  
7 health-related, and breath analysis disease diagnostics. A study for understanding the structure-  
8  
9 property relationship between the PAH corona and PAH substituent functionality and the VOC  
10  
11 chemical nature is underway and will be published elsewhere.  
12  
13  
14  
15  
16  
17  
18  
19  
20  
21  
22  
23  
24  
25  
26  
27  
28  
29  
30  
31  
32  
33  
34  
35  
36  
37  
38  
39  
40  
41  
42  
43  
44  
45  
46  
47  
48  
49  
50  
51  
52  
53  
54  
55  
56  
57  
58  
59  
60



1  
2  
3 **ASSOCIATED CONTENT**  
4

5  
6  
7 **AUTHOR INFORMATION**  
8

9 Corresponding Author (H.H): [hhossam@tx.technion.ac.il](mailto:hhossam@tx.technion.ac.il)  
10

11  
12  
13 **NOTES**  
14

15 The authors declare no competing financial interest.  
16  
17

18  
19 **ACKNOWLEDGMENTS**  
20

21 The research leading to these results has received partial funding from the FP7's ERC grant under  
22 DIAG-CANCER (grant agreement no. 256639). We acknowledge Mr. A'laa Garaa, Mr. Rawi  
23 Dirawi, Dr. Ulrike (Mirjam) Tisch, Dr. Greogory Shuster, Dr. Yael Zilberman, Ms. Nisreen  
24 Shehada (Technion IIT), Mr. Nadav Bachar and Dr. Radu Ionescu (Tarragona University) for  
25 assistance and fruitful discussions.  
26  
27  
28  
29  
30  
31  
32  
33  
34

35 **Supporting Information**  
36

37 Scanning electron microscopy images of FET surfaces of the different PAHs after the exposure  
38 experiments; non-normalized sensing features on increasing the concentration of ethylbenzene in  
39 5% RH as a function of time; accuracy of discrimination between various groups and various  
40 types of VOCs, using different combinations of sensors and electrical features. This material is  
41 available free of charge via the Internet at <http://pubs.acs.org>.  
42  
43  
44  
45  
46  
47  
48  
49  
50  
51  
52  
53  
54  
55  
56  
57  
58  
59  
60

**REFERENCES:**

- (1) Wallace, L.; Pellizzari, E.; Leaderer, B.; Zelon, H.; Sheldon, L. *Atmosph. Environm.* **1987**, 21, 385-393.
- (2) Guo, H.; Lee, S.; Chan, L.; Li, W. *Environ Res.* **2004**, 94, 57-66.
- (3) Hakim, M.; Broza, Y. Y.; Barash, O.; Peled, N.; Phillips, M.; Amann, A.; Haick, H. *Chem. Rev.* **2012**, 112, 5949-5966.
- (4) Tisch, U.; Billan, S.; Ilouze, M.; Phillips, M.; Peled, N.; Haick, H. *CML - Lung Cancer* **2012**, 5, 107-117.
- (5) Tisch, U.; Haick, H. *Rev. Chem. Eng.* **2010**, 26, 171-179.
- (6) Peled, N.; Hakim, M.; Tisch, U.; Bunn, P. A. J. R.; Miller, Y. E.; Kennedy, T. C.; Mattei, J.; Mitchell, J. D.; Weyant, M. J.; Hirsch, F. R.; Haick, H. *J. Thorac. Oncol.* **2012**, 7, 1528-1533.
- (7) Peng, G.; Hakim, M.; Broza, Y. Y.; Billan, S.; Abdah-Bortnyak, R.; Kuten, A.; Tisch, U.; Haick, H. *Br. J. Cancer* **2010**, 103, 542-551.
- (8) Peng, G.; Tisch, U.; Adams, O.; Hakim, M.; Shehada, N.; Broza, Y. Y.; Billan, S.; Abdah-Bortnyak, R.; Kuten, A.; Haick, H. *Nature Nanotech.* **2009**, 4, 669-673.
- (9) Hakim, M.; Billan, S.; Tisch, U.; Peng, G.; Dvorkind, I.; Marom, O.; Abdah-Bortnyak, R.; Kuten, A.; Haick, H. *Br. J. Cancer* **2011**, 104, 1649-1655.
- (10) Barash, O.; Peled, N.; Tisch, U.; Bunn, P. A.; Hirsch, F. R.; Haick, H. *Nanomedicine (New York, NY, US)* **2012**, 8, 580-589.
- (11) Barash, O.; Peled, N.; Hirsch, F. R.; Haick, H. *Small* **2009**, 5, 2618-24.
- (12) Amal, H.; Ding, L.; Liu, B. B.; Tisch, U.; Xu, Z.-Q.; Shi, D.-Y.; Zhao, Y.; Chen, J.; Sun, R.-X.; Liu, H.; Ye, S. L.; Tang, S. L.; Haick, H. *Int. J. Nanomedicine* **2012**, 7, 4135-4146.
- (13) Haick, H.; Hakim, M.; Patrascua, M.; Levenberg, C.; Shehada, N.; Nakhoul, F.; Abassi, Z. *ACS Nano* **2009**, 3, 1258-1266.
- (14) Marom, O.; Nakhoul, F.; Tisch, U.; Shiban, A.; Abassi, Z.; Haick, H. *Nanomedicine (London, UK)* **2012**, 7, 639-650.

- 1  
2  
3 (15) Tisch, U.; Aluf, A.; Ionescu, R.; Nakhle, M.; Bassal, R.; Axelrod, N.; Robertman, D.; Tessler, Y.;  
4  
5 Finberg, J. P. M.; Haick, H. *ACS Chem. Neurosci.* **2012**, 3, 161-166.  
6  
7 (16) Tisch, U.; Schlesinger, I.; Ionescu, R.; Nassar, M.; Axelrod, N.; Robertman, D.; Tessler, Y.;  
8  
9 Marmur, A.; Aharon-Peretz, J.; Haick, H. *Nanomedicine (London, UK)* **2013**, 8(1), 43-56.  
10  
11 (17) Ionescu, R.; Broza, Y.; Shaltieli, H.; Sadeh, D.; Zilberman, Y.; Feng, X.; Glass-Marmor, L.;  
12  
13 Lejbkowicz, I.; Müllen, K.; Miller, A.; Haick, H. *ACS Chem. Neurosci.* **2011**, 2, 687-693.  
14  
15 (18) Tisch, U.; Haick, H. *MRS Bull.* **2010**, 35, 797-803.  
16  
17 (19) Konvalina, G.; Haick, H. *ACS Appl. Mater. Interf.* **2012**, 4, 317-325  
18  
19 (20) Bondavalli, P.; Legagneux, P.; Pribat, D. *Sens. Actuat. B* **2009**, 140, 304-318.  
20  
21 (21) Vlachos, D. S.; Skafidas, P. D.; Avaritsiotis, J. N. *Sens. Actuat. B* **1995**, 25, 491-494.  
22  
23 (22) Li, D.; Borkent, E. J.; Nortrup, R.; Moon, H.; Katz, H.; Bao, Z. *Appl. Phys. Lett.* **2005**, 86, 042105  
24  
25 1-3.  
26  
27 (23) Pacher, P.; Lex, A.; Eder, S.; Trimmel, G.; Slugovc, C.; List, E.; Zojer, E. *Sens. Actuators, B*  
28  
29 **2010**, 145, 181-184.  
30  
31 (24) Righettoni, M.; Tricoli, A.; Gass, S.; Schmid, A.; Amann, A.; Pratsinis, S. *Anal. Chim. Acta* **2012**,  
32  
33 738, 69-75.  
34  
35 (25) Potyrailo, R.; Nagraj, N.; Surman, C.; Boudries, H.; Lai, H.; Slocik, J. M.; Kelley-Loughnane, N.;  
36  
37 Naik, R. R. *Trends Anal. Chem.* **2012**, 40, 133-145.  
38  
39 (26) Bachar, N.; Mintz, L.; Zilberman, Y.; Ionescu, R.; Feng, X.; Müllen, K.; Haick, H. *ACS Appl.*  
40  
41 *Mater. Interf.* **2012**, 4, 4960-4965.  
42  
43 (27) Zilberman, Y.; Ionescu, R.; Feng, X.; Mullen, K.; Haick, H. *ACS Nano* **2011**, 5, 6743-6753  
44  
45 (28) Zilberman, Y.; Tisch, U.; Pisula, W.; Feng, X.; Mullen, K.; Haick, H. *Langmuir* **2009**, 25, 5411-  
46  
47 5416.  
48  
49 (29) Zilberman, Y.; Tisch, U.; Shuster, G.; Pisula, W.; Feng, X.; Mullen, K.; Haick, H. *Adv. Mater.*  
50  
51 **2010**, 22, 4317-4320.  
52  
53 (30) Torsi, L.; Dodabalapur, A.; Savvatini, L.; Zambonin, P. G. *Sens. Actuators, B* **2000**, 67, 312-316.  
54  
55  
56  
57  
58  
59  
60

- 1  
2  
3 (31) Li, B.; Lambeth, D. N. *Nano Lett.* **2008**, 8, 3563-3567.  
4  
5 (32) Paska, Y.; Haick, H. *J. Phys. Chem. C* **2009**, 113, 1993-1997  
6  
7 (33) Paska, Y.; Haick, H. *Appl. Phys. Lett.* **2009**, 95, 233103/1.  
8  
9 (34) Paska, Y.; Haick, H. *J. Am. Chem. Soc.* **2010**, 132, 1774-1775  
10  
11 (35) Paska, Y.; Haick, H. *ACS Appl. Mater. Interf.* **2012**, 4, 2604-2617.  
12  
13 (36) Paska, Y.; Stelzner, T.; Assad, O.; Tisch, U.; Christiansen, S.; Haick, H. *ACS Nano* **2012**, 6, 335-  
14  
15 345.  
16  
17 (37) Paska, Y.; Stelzner, T.; Christiansen, S.; Haick, H. *ACS Nano* **2011**, 5, 5620-5626.  
18  
19 (38) Feng, X.; Pisula, W.; Kudernac, T.; Wu, D.; Linjie, Z.; Feyter, S.; Müllen, K. *J. Am. Chem. Soc.*  
20  
21 **2009**, 131, 4439-4448.  
22  
23 (39) Feng, X. L.; Pisula, W.; Zhi, L. J.; Takase, M.; Müllen, K. *Angew. Chem. Int. Ed.* **2008**, 47, 1703-  
24  
25 1706.  
26  
27 (40) Feng, X. L.; Liu, M. Y.; Pisula, W.; Takase, M.; Li, J. L.; Müllen, K. *Adv. Mater.* **2008**, 14, 2684-  
28  
29 2689.  
30  
31 (41) Bashouti, M. Y.; Tung, R. T.; Haick, H. *Small* **2009**, 5, 2761-2769.  
32  
33 (42) Tripp, C.; Hair, M. *Langmuir* **1992**, 8, 1961-1967.  
34  
35 (43) Haynes, W. M., *CRC Handbook of Chemistry and Physics, 91st Edition*. CRC Press: Boulder,  
36  
37 Colorado, 2010-2011.  
38  
39  
40  
41  
42  
43  
44  
45  
46  
47  
48  
49  
50  
51  
52  
53  
54  
55  
56  
57  
58  
59  
60

1  
2  
3 **TOC Figure:**

